Harvest season, high polluted season in East China

Harvest season, high polluted season in East China

Xin Huang[1], Yu Song[1], Mengmeng Li, Jianfeng Li and Tong Zhu

State Key Joint Laboratory of Environmental Simulation and Pollution Control, Department of
Environmental Science, Peking University, Beijing 100871, People's Republic of China

E-mail: huangxin831@pku.edu.cn and songyu@pku.edu.cn

Abstract

East China, a major agricultural zone with a dense population, suffers from severe air
pollution during June, the agricultural harvest season, every year. Crop burning emits
tremendous amounts of combustion products into the atmosphere, not only rapidly degrading
the local air quality but also affecting the tropospheric chemistry, threatening public health and
affecting climate change. Recently, in mid-June 2012, crop fires left a thick pall of haze over
East China. We evaluated the PM_{10}, $PM_{2.5}$ (particulates less than 10 and 2.5 μm in
aerodynamic diameter) and BC (black carbon) emissions by analyzing detailed census data
and moderate resolution imaging spectroradiometer (MODIS) remote sensing images and then
simulated the consequent pollution using meteorological and dispersion models. The results
show that the crop fires sweeping from the south to the north are responsible for the intensive
air pollution during harvest season. It is necessary for scientists and governments to pay more
attention to this issue.

1. Introduction

Field burning of crop straws is common both in rural
agricultural regions and peri-urban areas in China which
is used to control weeds, reduce pests and clear land
inexpensively. The crop residues are generally burnt in large
piles. It could be an important source of atmospheric trace
gases and particulate matter (Jenkins *et al* 1992, Dennis *et al*
2002, Zhang *et al* 2008), including carbon dioxide (CO_2),
carbon monoxide (CO), methane (CH_4), non-methane organic
compounds (NMOCs), black carbon and organic carbon (BC
and OC), particulate matter (PM), etc. Crop fires also have
impact on atmospheric chemistry and global climate change
(Crutzen and Andreae 1990, Hobbs *et al* 1997, Thompson
et al 2001). In addition, short-term and long-term exposure to

PM, particularly BC, has been linked to adverse health effects,
including increased mortality, increased rates of hospital
admissions and emergency department visits, exacerbated
chronic respiratory conditions, and decreased lung function
(Fernandez *et al* 2001).

In China, a large agricultural country with the highest
crop production in the world, an estimated about 122 Tg
of crop residues are burned annually (Streets *et al* 2003).
East China, including the mid and lower reaches of the
Yangtze River and Yellow River, is a major agricultural
zone. It is a fertile region that's home to about one third
of China's cultivated land and almost half of the country's
agricultural yields. In recent decades, this region has also
become well known as one of the world's most robust
economic regions, with remarkable achievements and rapid
urbanization. Consequently, East China has now become
one of the most densely populated regions with large rural
and urban populations (about 0.6 billion people) (figure S1
available at stacks.iop.org/ERL/7/044033/mmedia). During
harvest season, East China is often reported to suffer from

[1] Authors to whom any correspondence should be addressed.

heavy regional air pollution. Particularly, in June 2012, a thick pall of haze was found over East China. Since 9 June, the measured PM_{10} concentration sharply increased in Hefei, Wuhan, Bozhou, Xuzhou and the surrounding areas. The government and public believe that crop fires may be the primary cause of this pollution; however, the actual source and accurate scope of pollution are still not known. A better understanding of crop fire emissions and their subsequent impact is required in order to improve air quality and reduce health risks. Here, we integrate field investigations, satellite observations and model simulations to qualify the impact of crop fires on regional pollution.

2. Method and data

2.1. Emission estimation and allocation

The emissions of $PM_{10}, PM_{2.5}$ and BC from crop fires in June were estimated based on crop production, residue-to-production ratio, percentage of crop residues burned in the field and combustion efficiency.

In this study, agricultural field burning emissions were initially estimated at a provincial level by multiplying the total mass of in-field burning crop residues and the corresponding emission factor (EF). The provincial amounts of crop residues burned in fields were estimated based on crop production using the following equation:

$$M_{i,k} = P_{i,k} \times R_k \times F_{i,k} \times CE_k$$

where, i for each province; k for different crop species; $M_{i,k}$ is provincial mass of crop residue burned in the field for crop species i; $P_{i,k}$ is provincial crop production for various crops; R_k is crop-specific residue-to-production ratio (dry matter); $F_{i,k}$ is province and crop-specific percentage of crop residues burned in fields; CE_k is crop-specific combustion efficiency.

Provincial-level crop production data for China referred to China Rural Statistical Yearbook distributed by the National Bureau of Statistics of China (NBSC 2012). And the residue-to-production ratios on dry matter basis in this estimation were based on previous study (Lal 2005). A questionnaire survey was carried out among rural families in Anhui, Shandong, Henan and Hubei province in order to better understand the current status of crop burning in East China. The values of percentage of crop residues burned in fields were adopted from our investigation on the usage of crop residues. Combustion efficiencies specified by crop type were collected based on existing publications (Turn *et al* 1997, de Zarate *et al* 2005). $PM_{10}, PM_{2.5}$ and BC from crop fires were calculated as a product of crop-specific burned mass and corresponding EFs. The emission factors for different pollutants were based on Li *et al*'s study (2007).

MODIS Thermal Anomalies/Fire Daily L3 Global Product (MOD/MYD14A1) for June 2012 was used for the allocation, which provides data from both the Terra and Aqua satellites. The enhanced contextual fire detection algorithm was used MODIS Thermal Anomalies/Fire products through brightness temperatures derived from the MODIS 4 and 11 mm channels. The fire detection strategy was based on absolute detection of the fire, if the fire is strong enough, and on detection relative to the thermal emission of surrounding pixels to detect weaker fires. The product is tile-based, with each product file spanning one of the 460 MODIS tiles, of which 326 contain land pixels, and in 1 km gridded cell over each daily (24 h) compositing period. Two observations per day are possible with the Terra overpass at 10:30 local time and the Aqua overpass at 14:30 local time.

The emissions in ith grid (E_i) were calculated using the following equation:

$$E_i = \frac{FC_i}{FC_k} \times E_k$$

where FC_i is the fire counts in ith grid, FC_k is the total fire counts in province k, and E_k is the total emissions from crop residue burning in province k.

2.2. Model configurations

The impact of crop fire emissions on atmospheric pollutant concentrations was simulated by combining the Weather Research and Forecasting (WRF) Model and the advanced non-steady-state air quality model (CALPUFF).

WRF version 3.3.1 released in September 2011 was applied to provide meteorological forecasts in our study. Accurate simulations of meteorological fields are important for pollutant transport. However, several key land-surface parameters in WRF are outdated. By default, WRF uses the USGS global land-use data derived from the AVHRR (Advanced Very High Resolution Radiometer) observation, which is based on 1 yr data from April 1992 to March 1993. However, over the last decade, global terrestrial ecosystems, particularly East China, underwent great changes, such as urbanization, desertification and deforestation, causing the existing USGS land-use data to be inaccurate (Pielke *et al* 2002). Consequently, MODIS land-use data (MCD12Q1) for the year 2006 and water mask data (MOD44W) for the year 2000, which both have a resolution of 500 m (Justice *et al* 2002), were introduced to obtain a new land-use map in our study. In addition, currently the vegetation fraction (VGF) dataset used in WRF is derived from 5 yr NDVI (Normalized Difference Vegetation Index) data at 0.144° resolutions from the AVHRR (Miller *et al* 2006). In this simulation, the VGF was updated by recalculating MODIS NDVI data (MOD13A2, monthly NDVI at 1 km resolution).

The advanced mesoscale WRF was set up to simulated fields of meteorological variables initially over a larger domain with horizontal resolution 27 km × 27 km which was subsequently nested down to a smaller domain of 9 km × 9 km resolution centered at 34.0°N, 117.5°E. From the ground level to the top pressure of 50 hPa, there were 27 vertical sigma layers to all grid meshes. The initial meteorological fields and boundary conditions are from NCEP global reanalysis data with 1° × 1° resolution. WRF was run for the entire month of June 2012, and each run covered 3.5 days with 12 h spin-up time. The domain settings and configuration options are presented in table 1.

CALPUFF (Version 6.42) is the USEPA's regulatory model for assessing long range transport of pollutants and

Table 1. WRF domain setting and configuration options and CALPUFF area source parameters.

WRF domain setting and configuration options		
	Domain 1	Domain 2
Horizontal grid (*x*, *y*)	80, 80	121, 121
Grid spacing	27 km	9 km
Microphysics	WRF single-moment 3-class scheme	
Long-wave radiation	RRTM scheme	
Short-wave radiation	Dudhia scheme	
Land-surface	Noah land-surface model	
Boundary layer	Yonsei University scheme	
Cumulus parameterization	Kain–Fritsch scheme	
Area source parameters in CALPUFF		
Temporal variations of the emissions	Emitted from 10:00 A.M. to 10:00 P.M.	
Effective height of area source	0.8 m	
Temperature	400 K	
Effective rise velocity	1.0 m s^{-1}	

their impacts. The refined meteorological data in WRF was used as input to drive the CALPUFF modeling system to predict hourly concentrations of PM. Only the crop fires emissions were considered in this study. All the fire emissions were treated as square area source with side length of 1 km. More detailed information is shown in table 1.

3. Results and discussion

3.1. Spatiotemporal distributions of crop fires

The occurrence of fires could be detected by the MODIS Thermal Anomalies and Fire Daily product (MOD/MYD14A1) with a 1 km resolution. The fire distribution and daily variations during 1 June–24 June are presented in figure 1. As shown in this figure, regional crop fires were mostly in eastern Henan province, southern Shandong province, northern Anhui province, and northern Jiangsu province (figure 1(A)). On the basis of our questionnaire carried out in 4 provinces in East China, we determined that the crop fires in June were specifically related to burning wheat and rapeseed straws. Both wheat and rapeseed are sown around mid-October and reaped at the end of May or the beginning of June. Spatially, wheat is most wildly cultivated in Hebei, Henan, Shandong and Anhui province (about 76 Tg annually, accounting for China's 66% wheat production). Rapeseed is primarily concentrated in Hubei, Anhui and Jiangsu province (NBSC 2012). Just after the harvest of wheat and rapeseed, straws are burnt in the fields to clear land for subsequent cultivation, thereby bringing about large-scale crop fires.

Temporally, the burning began on a large-scale since 8 June, peaked on 9 and 13 June, and subsided after 14 June (figure 1(B)). During this period, crop fires generally swept from the south to the north. Initially, the fires were mostly located in north-central Anhui and south Henan. On 9 June, the high temperature and sunshine facilitated crop burning activities, leading to large-scale fires in Anhui, Jiangsu,
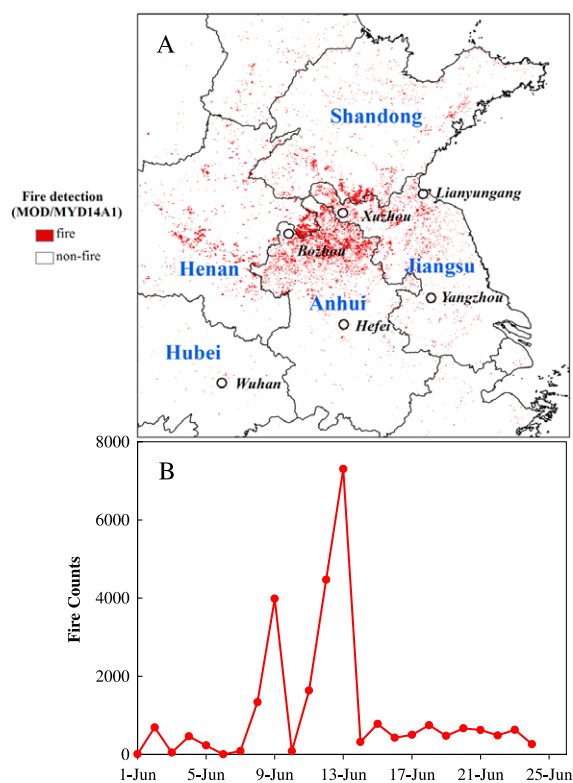

Figure 1. Spatial distribution (A) and temporal variation (B) of crop fires in June 2012. (Cities are marked in black with open circles; provinces are labeled in blue.)

Shandong, Henan and Hebei. The occurrence of fires dropped suddenly on 10 and 11 June, as a result of precipitation and the thick cloud cover, which both decreased the crop burning activities and affected the fire detection. After 12 June, the rain stopped, and the crop fires became intensive again as a result of the improved weather conditions. On 12 June, fires were crowded in eastern Henan and Hubei province. On 13 June, as many as 7304 fires count of was captured, most of which were located in eastern Henan, northern Anhui and Jiangsu. After 14 June, the crop fires ceased gradually, bringing an end to these successive regional pollution episodes.

3.2. Provincial and crop-specific emissions

In June 2012, about 0.2 Tg PM$_{2.5}$ and 26 Gg BC in total were released into the atmosphere in East China. Province-specific emissions are listed in table 2. Emissions were most concentrated in Henan province (65.9 Gg PM$_{2.5}$ and 6.5 Gg BC), followed by Shandong province (40.6 Gg PM$_{2.5}$ and 4.0 Gg BC).

Henan and Shandong province have highest agriculture production in China, which is primarily attributed to large wheat cultivation. In Anhui and Jiangsu province, besides wheat straws, rapeseed straws burning also play an important role, contributing about 40% of total emissions. While in Hubei province, emissions were mostly caused by rapeseed straws fires due to widely cultivated rapeseed. Crop residues have various usages in China's rural area, including fertilizer,
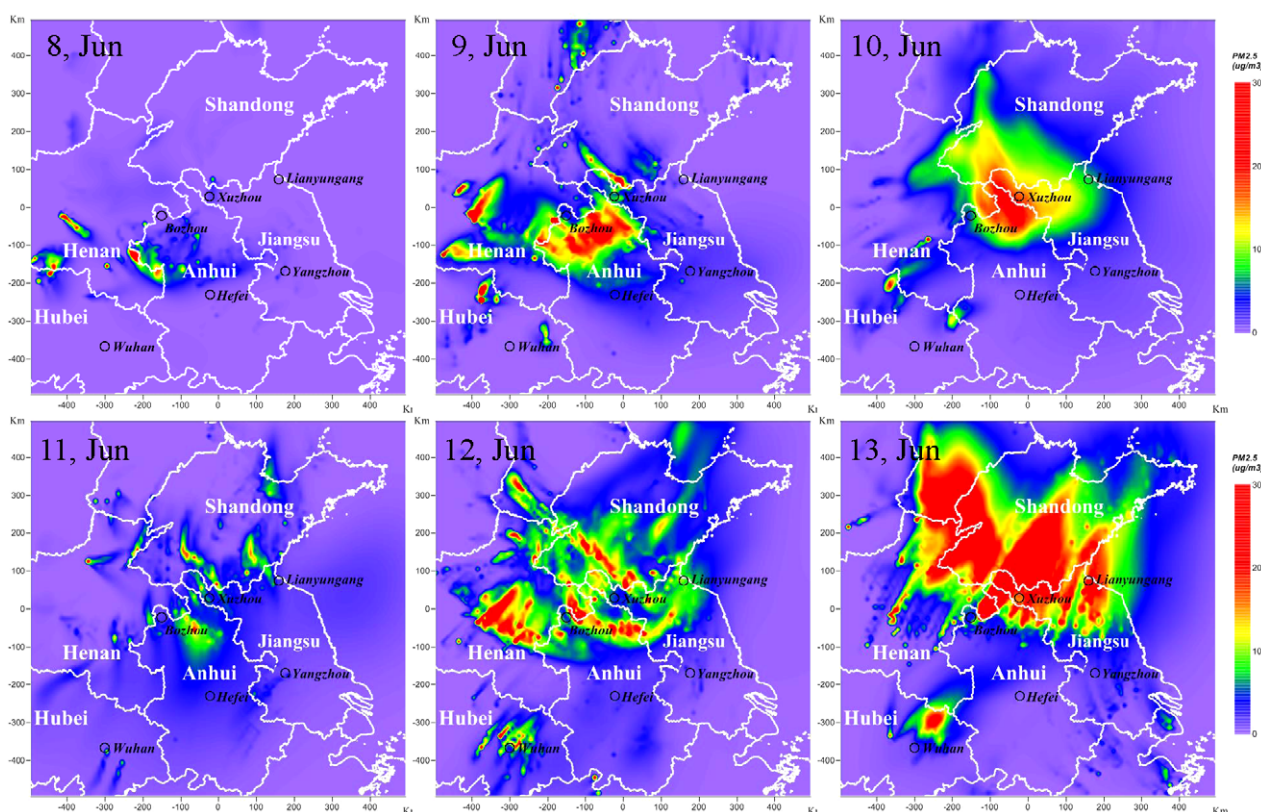
3

Figure 2. Modeled daily averaged $PM_{2.5}$ concentrations during 8–13 June 2012 in East China.

Table 2. Provincial level agricultural open fire emissions (Gg) in June 2012.

Province	PM_{10}		$PM_{2.5}$		BC	
	Wheat	Rapeseed	Wheat	Rapeseed	Wheat	Rapeseed
Anhui	24.1	8.5	23.7	8.3	2.3	0.8
Jiangsu	20.2	7.2	19.8	7.1	2.0	0.7
Hebei	24.6	0.2	24.1	0.2	2.4	0.02
Henan	61.7	5.7	60.4	5.5	6.0	0.5
Hubei	6.9	14.8	6.7	14.5	0.7	1.4
Shandong	41.2	0.2	40.4	0.2	4.0	0.02

fodder, fuel, raw material, burned in field, etc. According to our investigation on usage of crop residues, about 30% wheat straws and 50% rapeseed straws are burnt in field after harvest in 2011, more than the corresponding values in the year of 2000 (Yan *et al* 2006). This disparity could be attributed to fewer straws are used as biofuel with increasing income of rural families in recent years.

3.3. Modeled results and comparisons with observations

The emissions, transport and deposition of PM_{10}, $PM_{2.5}$ and BC relating to crop fires were simulated during 7–15 June. The predicted concentrations compared with measurements taken at nearby air quality ambient monitoring stations as well as satellite observations.

Since 8 June, when wheat and rapeseed straws were burned extensively, the regional air pollution became increasingly worse. As described in figure 2, initially, the

fires were mostly scattered in north-central Anhui and south Henan; thick fire smoke was only located on the border of these two provinces. Then on 9 June, the high temperature and sunshine facilitated crop burning activities, leading to large-scale fires in Anhui, Jiangsu, Shandong, Henan and Hebei. Together with the unfavorable meteorological conditions of low wind speed, the regional air quality degraded sharply in almost all of East China, especially northern Anhui, eastern Henan and southern Shandong (more detailed information on modeled meteorological data and detailed hourly observations are presented in figure S2 available at stacks.iop.org/ERL/7/044033/mmedia). Due to the intense fires emission and its transportation with southwesterly wind, severe pollution last until 10 June in southern Shandong, northeast Anhui and northwest Jiangsu. For instance, the simulated PM_{10} concentration in the city of Xuzhou increased from less than 10 $\mu g\ m^{-3}$ on 8 June to 62 $\mu g\ m^{-3}$ on 9 June and 158 $\mu g\ m^{-3}$ on 10 June.
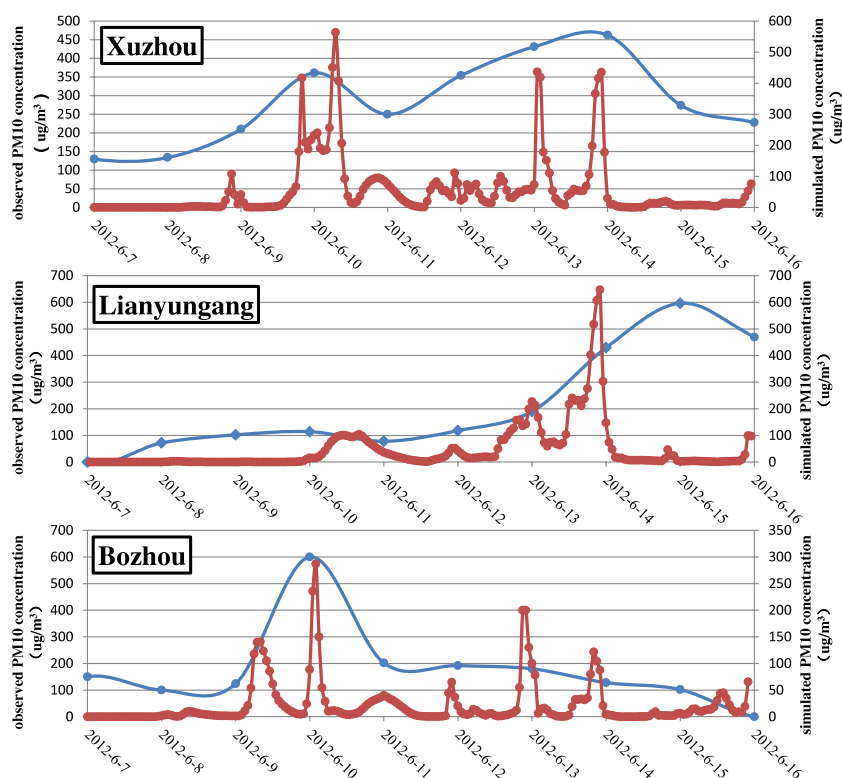
Figure 3. Comparison between PM_{10} observation (blue, daily averaged) and modeled PM_{10} (red, hourly averaged) concentrations during 7–15 June in Xuzhou, Lianyungang and Bozhou.

Correspondingly, measured PM_{10} concentration reached up to 210 μg m^{-3} and 361 μg m^{-3} on 9 and 10 June. Similarly, Bozhou also suffered dramatically increased PM_{10} concentration, exceeding 600 μg m^{-3} on 10 June. It is worth noting that the guideline values for 24 h mean concentrations of $PM_{2.5}$ and PM_{10} recommended by the World Health Organization (WHO) are only 25 and 50 μg m^{-3}, respectively (WHO 2006). The occurrence of fires dropped suddenly on 10 and 11 June, as a result of precipitation and the thick cloud cover, and consequently, the fire activities were slightly mitigated momentarily. Accordingly, the simulated and measured PM_{10} in Xuzhou decreased to 42.5 μg m^{-3} and 250 μg m^{-3} on 11 June. Comparison between PM_{10} observation and modeled PM_{10} concentrations are shown in figure 3. After 12 June, the rain stopped, and the crop fires became intensive again as a result of the improved weather conditions. Fires were crowded in eastern Henan, northern Anhui and southern Shandong. Smoke moved westerly, mainly affecting north Anhui and Jiangsu. On the same day, the city of Wuhan also suffered from increased air pollution, which was caused by circumjacent crop fires and unfavorable diffusion conditions. The modeled PM_{10} concentration results reached a peak of 156 μg m^{-3} on the night of 12 June. And observed PM_{10} concentration reached up to 373 μg m^{-3}, the highest value in recent years. The most severe pollution occurred on 13 June, as many as 7304 fires count of was captured, most of which were located in eastern Henan, northern Anhui and Jiangsu. Prevailing southwest winds transported the pollutants to north Jiangsu on 13 June and then northeast to Shandong province on 14

June. For the city of Lianyungang in Jiangsu province, the simulated daily averaged PM_{10} concentration on 13 June was 227 μg m^{-3}, about 53% of the observed PM_{10} concentration (429 μg m^{-3}), elevated by 125% compared with the previous day, as presented in figure 3. However, modeled PM_{10} concentration is significantly lower than observations on 14 June. It might be attributed to poorly-conceived atmospheric chemistry in CALPUFF or emission sources other than crop fires. Together with PM, tremendous VOCs were also emitted in the atmosphere during crop fires. Under favorable meteorological conditions, they could produce large amounts of SOA (secondary organic aerosols), contributing to high PM concentrations (Mauzerall *et al* 1998). Research on the atmospheric chemistry reactions during crop fires and emissions from other emission sources will be conduct in our further study by using chemical transport model to comprehensively understand the impact of crop fires. Our model results were also compared with the Aerosol Optical Depth (AOD) observations (MOD04 L2, collection 005). A comparison of the simulated and observed results for 13 June is shown in figure 4. Although dependent on cloud cover, the AOD data also indicated that north Jiangsu and west Shandong underwent the most severe pollution. After 14 June, the crop fires ceased gradually, bringing an end to these successive regional pollution episodes.

3.4. Interannual variability

As discussed above, crop fires were the foremost cause of the heavy pollution over East China during the middle of
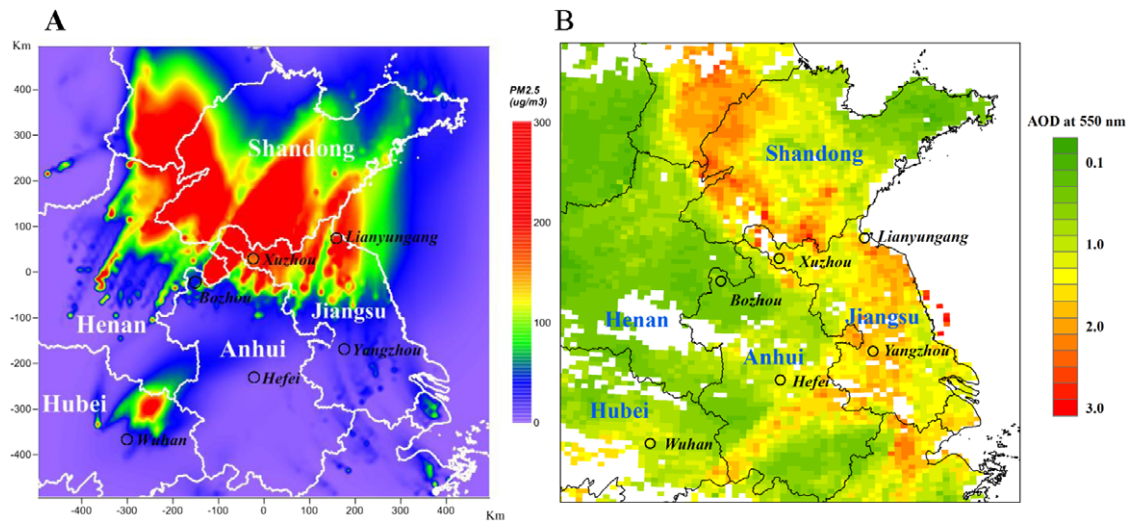
Figure 4. Comparison between modeled PM$_{2.5}$ (A) concentrations and AOD observation (B) on 13 June.
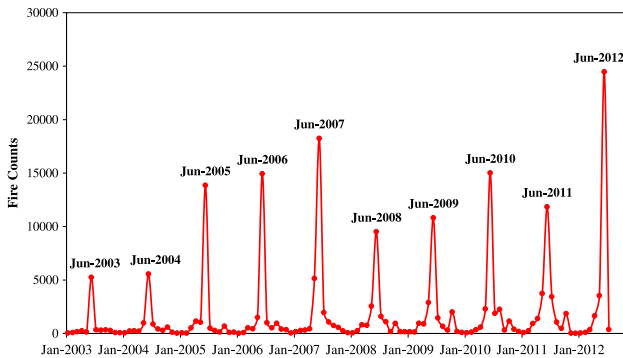

Figure 5. Temporal variation in the occurrence of crop fires during 2003–12 in East China.

June 2012. Moreover, instead of happenstance, this pollution spike occurs in China almost every year. A 10 yr time series of crop fires in East China, based on the MODIS Thermal Anomalies/Fire products (MOD/MYD14A1) and Global Land Cover 2000 for China (GLC-China), is presented in figure 5. Fires predominantly occur in the early and middle June, accounting for over 75% of fires annually. These observations are in general agreement with agricultural timing. Wheat–maize rotation systems are widely used in this area. Wheat is sown in mid-October and reaped at the end of May or the beginning of June, followed by and summer maize sown in mid-June and reaped in the end of September. Just after the harvest, wheat straws are burnt in the fields to clear land for subsequent maize cultivation. Therefore, every June, large-scale crop fires bring about regional air pollution.

3.5. Discussions

The common practice of pre- or post-harvest crop burning not only results in a loss of nutrients but also causes environmental pollution and associated health effects. According to our questionnaire survey, the practice of crop burning is associated with a variety of factors, such as a farmer's education level, level of agricultural mechanization, family income structure, and awareness of the harms of crop burning to the environment and human health. However, crop straw is still primarily disposed in traditional ways like field burning. Therefore, it is an urgent need to encourage alternatives to agricultural burning. More cost-effective crop straw utilization, such as biogas production, power generation and animal feed supply, should be promoted and generalized. It largely relies on a combination of technological development, economic policies and political interventions. Policy consideration is urgently required, both at the level of the province and central governments, to minimize crop burning and reduce its related health impact.

Acknowledgments

References

Crutzen P J and Andreae M O 1990 Biomass burning in the tropics—impact on atmospheric chemistry and biogeochemical cycles *Science* **250** 1669–78

Dennis A, Fraser M, Anderson S and Allen D 2002 Air pollutant emissions associated with forest, grassland, and agricultural burning in Texas *Atmos. Environ.* **36** 3779–92

de Zarate I O, Ezcurra A, Lacaux J P, Van Dinh P and de Argandona J D 2005 Pollution by cereal waste burning in Spain *Atmos. Res.* **73** 161–70

Fernandez A, Davis S B, Wendt J O L, Cenni R, Young R S and Witten M L 2001 Public health—particulate emission from biomass combustion *Nature* **409** 998

Hobbs P V, Reid J S, Kotchenruther R A, Ferek R J and Weiss R 1997 Direct radiative forcing by smoke from biomass burning *Science* **275** 1776–8

Jenkins B M, Turn S Q and Williams R B 1992 Atmospheric emissions from agricultural burning in California—

determination of burn fractions, distribution factors, and crop-specific contributions *Agric. Ecosyst. Environ.* **38** 313–30

Justice C, Townshend J, Vermote E, Masuoka E, Wolfe R, Saleous N, Roy D and Morisette J 2002 An overview of MODIS land data processing and product status *Remote Sens. Environ.* **83** 3–15

Lal R 2005 World crop residues production and implications of its use as a biofuel *Environ. Int.* **31** 575–84

Li X, Wang S, Duan L, Hao J, Li C, Chen Y and Yang L 2007 Particulate and trace gas emissions from open burning of wheat straw and corn stover in China *Environ. Sci. Technol.* **41** 6052–8

Mauzerall D L, Logan J A, Jacob D J, Anderson B E, Blake D R, Bradshaw J D, Heikes B, Sachse G W, Singh H and Talbot B 1998 Photochemistry in biomass burning plumes and implications for tropospheric ozone over the tropical South Atlantic *J. Geophys. Res.—Atmos.* **103** 8401–23

Miller J, Barlage M, Zeng X, Wei H, Mitchell K and Tarpley D 2006 Sensitivity of the NCEP/Noah land surface model to the MODIS green vegetation fraction data set *Geophys. Res. Lett.* **33** L13404

NBSC 2012 *China Statistical Yearbook 2011* (Beijing: China Statistics Press) (available at: www.stats.gov.cn/tjsj/ndsj/2011/indexeh.htm)

Pielke R A, Marland G, Betts R A, Chase T N, Eastman J L, Niles J O, Niyogi D D S and Running S W 2002 The influence of land-use change and landscape dynamics on the climate system: relevance to climate-change policy beyond the radiative effect of greenhouse gases *Phil. Trans. R. Soc.* A **360** 1705–19

Streets D G, Yarber K F, Woo J H and Carmichael G R 2003 Biomass burning in Asia: annual and seasonal estimates and atmospheric emissions *Glob. Biogeochem. Cycles* **17** 1099

Thompson A M, Witte J C, Hudson R D, Guo H, Herman J R and Fujiwara M 2001 Tropical tropospheric ozone and biomass burning *Science* **291** 2128–32

Turn S Q, Jenkins B M, Chow J C, Pritchett L C, Campbell D, Cahill T and Whalen S A 1997 Elemental characterization of particulate matter emitted from biomass burning: wind tunnel derived source profiles for herbaceous and wood fuels *J. Geophys. Res.—Atmos.* **102** 3683–99

WHO 2006 *Air Quality Guidelines: Global Update 2005: Particulate Matter, Ozone, Nitrogen Dioxide and Sulfur Dioxide* (Geneva: World Health Organization) (available at: http://whqlibdoc.who.int/hq/2006/WHO_SDE_PHE_OEH_06.02_eng.pdf)

Yan X Y, Ohara T and Akimoto H 2006 Bottom-up estimate of biomass burning in mainland China *Atmos. Environ.* **40** 5262–73

Zhang H F, Ye X N, Cheng T T, Chen J M, Yang X, Wang L and Zhang R Y 2008 A laboratory study of agricultural crop residue combustion in China: emission factors and emission inventory *Atmos. Environ.* **42** 8432–41